CHEMISTRY OF MATERIALS
Article

Chem. Mater. **2011,** *23,* 181–187 181
DOI:10.1021/cm102565y

Broken Band Alignment in EuS-CdS Nanoheterostructures

Tihana Mirkovic,[†] David Rossouw,[‡] Gianluigi A. Botton,*[,‡] and Gregory D. Scholes*[,†]

[†]*Lash-Miller Chemical Laboratories, University of Toronto, 80 St. George Street, Toronto, Ontario, Canada M5S 3H6, and* [‡]*Materials Science and Engineering, McMaster University, 1280 Main Street West, Hamilton, Ontario, Canada, L8S 4L8*

Received September 7, 2010. Revised Manuscript Received October 25, 2010

Integration of multiple materials in a controllably programmed manner on the nanoscale has led to the evolution of the next generation of nanoparticles. We have explored the formation of bifunctional europium sulfide − cadmium chalcogenide composite nanostructures, as both of the semiconductor materials exhibit intriguing physical characteristics, suggesting that architectural tunability of these hybrid structures could have interesting effects on their collective properties. A two step synthetic procedure has been devised, where CdSe or CdS nanorods were used as a platform for the growth of the secondary material domains. An eight-coordinate lanthanide based single-source precursor, $Eu(Ddtc)_3(Bipy)$, was implemented as the material source for the selective growth of spherical EuS nanocrystals on the tips of cadmium chalcogenide nanorods. The composition and structure of these hybrid particles have been analyzed by high-resolution TEM. The nanoheterostrucutre has a type III, or broken band alignment, which has led to the quenching of the luminescence of the initial cadmium chalcogenide nanorods following the growth of EuS tips and the formation of the interfacial heterojunction.

Introduction

Development of sophisticated colloidal chemical routes over the past decade has enabled the preparation of compositionally and morphologically intricate nanostructures. Diversity of properties has particularly been achieved through incorporation of multiple materials in a heterostructured nanocrystal.[1] As heterostructured nanoparticles are comprised of distinct material domains, each characterized with their specific physical properties, surface chemistry, and morphology, they present model systems for investigations of interactions between different nanoscale components. Modification of properties of the individual moieties as a result of the coupling between the two different domains is often observed to originate through interactions at the shared interface, which might lead to energy, spin and charge transfer.[2−6] Enhancement or modulation of physical properties resulting from heterostructure architectures are becoming more common, but realization of true multifunctionality in hybrid particles poses still a challenge. Bifunctional nanocomposites could be very attractive for a broad range of applications as compared to homogeneous nanoparticles. For example in the areas of multifunctional biolabeling,[7,8] materials have been explored that incorporate a magnetic core covered with a luminescent shell composed of either dye-impregnated silica or CdSe. Here we report an example of a heteronanostructure which incorporates a europium sulfide domain, known to exhibit size-dependent magnetic properties at the nanoscale,[9] such as superparamagnetism previously reported in Mn/CdSe quantum dots,[10] and a cadmium chalcogenide moiety, a material well studied for its photophysical characteristics. In particular, we focus on the development of the synthetic methodology based on a single-source precursor, the structural characterization of the nanocrystalline material and the resulting optical properties of the EuS-CdS heterostructures.

Flexibility in the synthetic methodologies and tunability of reaction conditions led to the realization of morphologically distinct heterostructures classified on the basis of the relative position of the integrated materials. Architectures have been found to range between centrosymmetric core/shell geometries,[11,12]

*E-mail: gbotton@mcmaster.ca (G.A.B.). E-mail: gscholes@chem.utoronto.ca. Corrresponding author address: Department of Chemistry, Institute for Optical Sciences University of Toronto 80 St. George Street, Toronto, Ontario M5S 3H6, Canada (G.D.S.).

(1) Lo, S.; Mirkovic, T.; Chuang, C.-H.; Burda, C.; Scholes, G. D. *Adv. Mater.* **2010**, accepted.
(2) Zeng, H.; Li, J.; Liu, P. P.; Wang, Z. L.; Sun, S *Nature* **2002**, *420*, 395.
(3) Kumar, S.; Jones, M.; Lo, S. S.; Scholes, G. D. *Small* **2007**, *3*, 1633.
(4) He, J.; Zhong, H. Z.; Scholes, G. D. *Phys. Rev. Lett.* **2010**, 046601.
(5) Chuang, C.-H.; Lo, S. S.; Scholes, G. D.; Burda, C. *J. Phys. Chem. Lett.* **2010**, *1*, 2530.
(6) Dooley, C. J.; Dimitrov, S. D.; Fiebig, T. *Phys. Chem. C* **2008**, *112*, 12074.
(7) Kim, H.; Achermann, M.; Balet, L. P.; Hollingsworth, J. A.; Klimov, V. I. *J. Am. Chem. Soc.* **2005**, *127*, 544.
(8) Lu, Y.; Yin, Y.; Mayers, B. T.; Xia, Y. *Nano Lett.* **2002**, *2*, 183.
(9) Zhao, F.; Sun, H.-L.; Gao, S.; Su, G. *J. Mater. Chem.* **2005**, *15*, 4209–4214.
(10) Magnana, D.; Perera, M. D.; Harter, A. G.; Dalal, N. S.; Strouse, G. F. *J. Am. Chem. Soc.* **2006**, *128*, 2931.
(11) Kim, S.; Fisher, B.; Eisler, H.-J.; Bawendi, M. *J. Am. Chem. Soc.* **2003**, *125*, 11466.
(12) Ivanov, S. A.; Piryatinski, A.; Nanda, J.; Tretiak, S.; Zavadil, K. R.; Wallace, W. O.; Werder, D.; Klimov, V. I. *J. Am. Chem. Soc.* **2007**, *129*, 11708.

Published on Web 12/22/2010

heterodimers[13,14] to more elaborate multicomponent anisotropic particles such as nanorods,[3,15,16] barbells,[17−22] tetrapods[23,24] and multibranched nanocrystals.[25] Typically, heterostructures can be synthesized either through sequential growth of the secondary domain onto preformed nanocrystals[17,20,26] or alternatively through a one-pot synthetic approach[27,28] which allows for growth of two separate particle moieties. A rich diversity in material composition has also been achieved, where some of the most explored semiconductor combinations include CdSe/ZnS,[29] CdSe/ZnSe,[30] CdTe/CdSe,[11,31] ZnTe/CdS,[32] and ZnSe/CdS.[33] Additionally, Banin and co-workers[20] demonstrated the formation of CdSe nanorods and tetrapods decorated with gold nanoparticles, whereas heterostructures comprised of semiconductor and magnetic nanocomponents, including CdSe-Co,[7] CdS-FePt,[26] and γ-Fe_2O_3-metal sulfides,[34] have also been recently fabricated.

Several studies of nanocrystalline europium chalcogenides have been reported over the past five years, as the potential of those materials for ferromagnetic semiconductors, or as systems displaying spintronic or optoelectronic phenomena, has been recognized.[35−37] We developed a single-source synthetic route for the preparation of high quality EuS nanocrystals[38,39] that has enabled studies on the optical and magnetic properties exhibited by this system.[9,40,41] To date, only monocomponent nanoparticles of EuS have been synthesized, but in the current work, we have explored hybrid formation of EuS-CdS composites, as both of the semiconductor materials exhibit intriguing physical properties. The two step synthetic methodology employs a high-temperature thermolysis of the single-source lanthanide precursor for the selective growth of EuS tips on preformed cadmium chalcogenide particles. Although limited in terms of possible reaction parameters, due to the high precursor decomposition temperature, it presents one of the rare examples where single-source precursors have been utilized in nanoheterostructure formation. EuS-CdS nanoparticles have been obtained either from the growth of EuS tips on CdSe nanorods, which during the synthesis undergo anion exchange, or directly by depositing EuS onto the tips of CdS nanorods. Structural analysis of the bifunctional nanocomposites has revealed crystalline domains of both materials, whereas the luminescence of the CdS stem has been observed to diminish following the evolution of secondary EuS moieties.

Experimental Section

Synthesis of Eu(Ddtc)$_3$(Bipy). The heteroligand lanthanide complex, utilized in the preparation of nanocrystalline EuS, was prepared following previously described synthetic procedures.[42−44] A solution of 2,2′-bipyridine monohydrate (> 99%, Aldrich), (0.64 g in 40 mL of boiling water) was added to an aqueous solution of $EuCl_3 \cdot 6H_2O$ (1.34 g, in 40 mL) (99.9%, Strem) under vigorous stirring. Drop-wise addition of a sodium diethyldithiocarbamate [Na(Ddtc)$\cdot H_2O$] (Sigma Aldrich) solution (2.7 g in 80 mL of water) to the above mixture resulted in a deep orange-red colored solid precipitate [Eu(Ddtc)$_3$(Bipy)], which was filtered and dried in vacuo at room temperature.

Synthesis of CdSe Nanorods. For the preparation of CdSe nanorods, a mixture of trioctylphosphine oxide (TOPO) (3.2 g), tetradecylphosphonic acid (TDPA) (0.64 g), and cadmium oxide (CdO) (0.102 g) was degassed at 100 °C and subsequently heated to 340 °C. 1.8 mL of trioctylphosphine (TOP) was injected after CdO cleared. Selenium was supplied in the form of Se: TOP (0.158 mL, 1 M) through a quick injection into the hot surfactant mixture under vigorous stirring at 300 °C. The growth process took place at 300 °C for 5 min under inert conditions. Following the synthesis, the rods were precipitated from the solution through the addition of methanol and ethyl acetate, while the CdSe precipitate was collected by centrifugation and finally dissolved in toluene for further analysis. The formed nanorods can be seen in Figure 1b.

Synthesis of CdS Nanorods. CdS nanorods were prepared by heating a mixture of 3.0 g of TOPO, 0.45 g of TDPA, and 0.21 g of CdO to 100 °C, at which point it was degassed for 30 min. The temperature was then increased to 320 °C and once the solution cleared, 2 mL of TOP was injected. The temperature was then decreased to 300 °C, when sulfur was introduced through a

(13) Yu, H.; Chen, M.; Rice, P. M.; Wang, S. X.; White, R. L.; Sun, S. *Nano Lett*. **2005**, *5*, 379–382.
(14) Pellegrino, T.; Fiore, A.; Carlino, E.; Giannini, C.; Cozzoli, P. D.; Ciccarella, G.; Respaud, M.; Palmirotta, L.; Cingolani, R.; Manna, L. *J. Am. Chem. Soc*. **2006**, *128*, 6690–6698.
(15) Milliron, D.; Hughes, S. M.; Cui, Y.; Manna, L.; Lin-Wang, J. L.; Alivisatos, A. P. *Nature* **2004**, *430*, 190.
(16) Hewa-Kasakarage, N. N.; El-Khoury, P. Z.; Schmall, N.; Kirsanova, M.; Nemchinov, A.; Tarnosky, A. N.; Bezryadin, A.; Zamkov, M. *Appl. Phys. Lett*. **2009**, *94*, 133113.
(17) Kirsanova, M.; Nemchinov, A.; Hewa-Kasakarage, N. N.; Schmall, N.; Zamkov, M. *Chem. Mater*. **2009**, *21*, 4305.
(18) Halpert, J. E.; Porter, V. J.; Zimmer, J. P.; Bawendi, M. G. *J. Am. Chem. Soc*. **2006**, *128*, 12590.
(19) Saunders, A. E.; Koo, B.; Wang, X.; Shih, C.-K.; Korgel, B. A. *Chem. Phys. Chem*. **2008**, *9*, 1158.
(20) Mokari, T.; Rothenberg, E.; Popov, I.; Costi, R.; Banin, U. *Science* **2004**, *304*, 1787.
(21) Kudera, S.; Carbone, L.; Casula, M. F.; Cingolani, R.; Falqui, A.; Snoeck, E.; Parak, W. J.; Manna, L. *Nano Lett*. **2005**, *5*, 445.
(22) Mokari, T.; Sztrum, C. G.; Salant, A.; Rabani, E.; Banin, U. *Nat. Mater*. **2005**, *4*, 855.
(23) Fiore, A.; Mastria, R.; Lupo, M. G.; Lanzani, G.; Giannini, C.; Carlino, E.; Morello, G.; De Giorgi, M.; Li, Y.; Cingolani, R.; Manna, L. *J. Am. Chem. Soc*. **2009**, *131*, 2274.
(24) Xie, R.; Kolb, U.; Basche, T. *Small* **2006**, *2*, 1454.
(25) Zhong, H.; Scholes, G. D. *J. Am. Chem. Soc*. **2009**, *131*, 9170.
(26) He, S.; Zhang, H.; Delikanli, S.; Qin, Y.; Swihart, M. T.; Zeng, H. *J. Phys. Chem. C* **2009**, *113*, 87.
(27) Lee, W.-R.; Kim, M. G.; Choi, J.-R.; Park, J.-I.; Ko, S. J.; Oh, S. J.; Cheon, J. *J. Am. Chem. Soc*. **2005**, *127*, 16090.
(28) Choi, S.-H.; Kim, E.-G.; Hyeon, T. *J. Am. Chem. Soc*. **2006**, *128*, 2520.
(29) Hines, M. A.; Guyot-Sionnest, P. *J. Phys. Chem*. **1996**, *100*, 468.
(30) Reiss, P.; Bleuse, J.; Pron, A. *Nano Lett*. **2002**, *2*, 781.
(31) Dorfs, D.; Franzl, T.; Osovsky, R.; Brumer, M.; Lifshitz, E.; Klar, T. A.; Eychmuller, A. *Small* **2008**, *8*, 1148.
(32) Xie, R. G.; Zhong, X. H.; Basche, T. *Adv. Mater*. **2005**, *17*, 2741.
(33) Nemchinov, A.; Kirsanova, M.; Hewa-Kasakarage, N. N.; Zamkov, M. *J. Phys. Chem. C* **2008**, *112*, 9301.
(34) Kwon, K.-W.; Shim, M. *J. Am. Chem. Soc*. **2005**, *127*, 10269.
(35) Hao, X.; Moodera, J. S.; Meservey, R. Spin. *Phys. Rev. B* **1990**, *42*, 8235–8243.
(36) Bohn, H. G.; Kollmar, A.; Zinn, W. *Phys. Rev. B* **1984**, *30*, 6504–6513.
(37) Tanaka, K.; Tatehata, N.; Fujita, K.; Hirao, K. *J. Appl. Phys*. **2001**, *89*, 2213–2219.
(38) Mirkovic, T.; Hines, M. A.; Nair, P. S.; Scholes, G. D. *Chem. Mater*. **2005**, *17*, 3451–3456.
(39) Huxter, V. M.; Mirkovic, T.; Nair, S. P.; Scholes, G. D. *Adv. Mater*. **2008**, *20*, 2439–2443.
(40) Regulacio, M. D.; Bussmann, K.; Lewis, B.; Stoll, S. L. *J. Am. Chem. Soc*. **2006**, *128*, 11173–11179.
(41) Redigolo, M. L.; Koktysh, D. S.; Rosenthal, S. J.; Dickerson, J. H.; Gai, Z.; Gao, L.; Shen, J. *Appl. Phys. Lett*. **2006**, *89*, 222501–3.
(42) Mirkovic, T.; Hines, M. A.; Nair, P. S.; Scholes, G. D. *Chem. Mater*. **2005**, *17*, 3451.
(43) Ivanov, R. A.; Korsakov, I. E.; Formanovskii, A. A.; Paramonov, S. E.; Kuz'mina, N. P.; Kaul', A. R. *Russ. J. Coord. Chem*. **2002**, *28*, 670.
(44) Ivanov, R. A.; Korsakov, I. E.; Kuzmina, N. P.; Kaul, A. R. *Mendeleev Commun*. **2000**, *2*, 83.

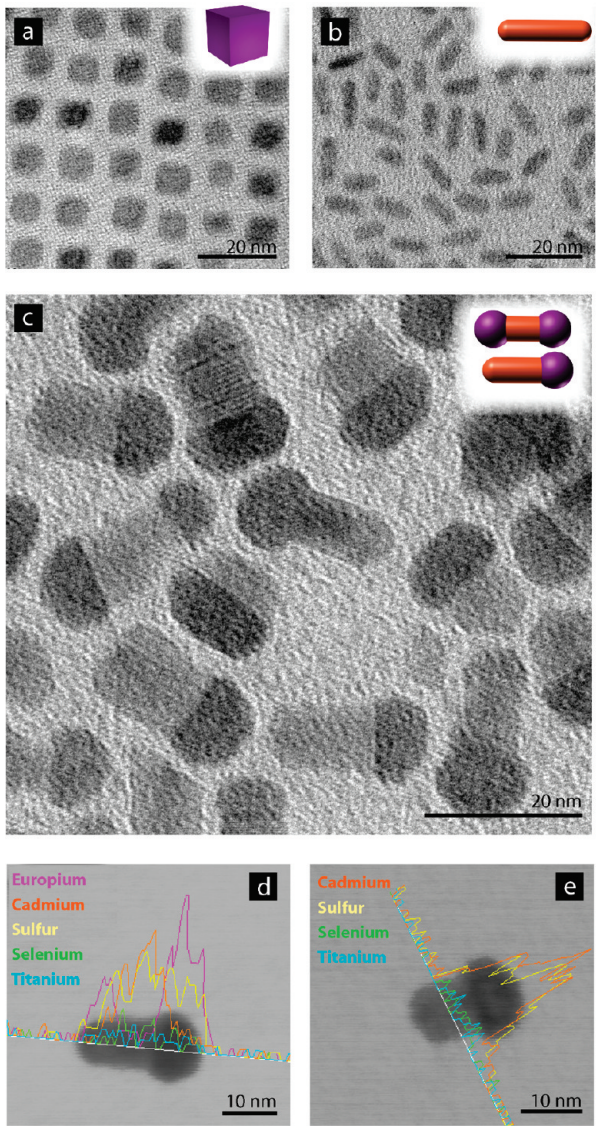

Figure 1. TEM micrographs of EuS cubes (a), CdSe nanorods (b), and the resulting EuS-CdS heterostructures (c) formed upon the addition of EuS precursor to preformed anisotropic CdSe nanocrystals (from b). Ion-exchange during the growth of EuS tips transforms the central region from CdSe to CdS. SEM images and EDX line scans (d) along the long axis and across (e) the CdS portion of the EuS-CdS heterostructure. Titanium does not appear in the particle and is just used as a baseline reference.

quick injection of 0.13 g of S in 2 mL of TOP. Growth of CdS nanorods occurred for 10 min to yield a bright yellow sample. The solid was collected through precipitation in methanol and ethyl acetate followed by centrifugation, upon which it was redispersed in toluene.

Synthesis of EuS-CdS Nanoheterostructures. The synthetic approach to the formation of EuS-CdS nanostructures was based on a drop-by-drop injection of the EuS single-source precursor into the solution of preformed CdSe nanorods at higher temperature. Initially 0.6 g of previously prepared CdSe nanorods (not purified) was placed in 2.0 mL of octadecene, and the mixture was heated to 300 °C under argon, at which point a slurry of $Eu(Ddtc)_3(Bipy)$ (0.4 g) in 2.0 mL of oleylamine was injected drop-by-drop into the hot solution. The temperature was dropped to 280 °C, and the reaction took place for an additional 10 min. Following the reaction termination, the heterostructures were isolated through precipitation with methanol and ethyl acetate and subsequent centrifugation. The sample was redispersed in toluene for further characterization. The resulting heterostructures can be seen in Figure 1c.

Alternatively, the heterostructures were also grown from initially prepared CdS nanorods following the exact procedure described above (see Supporting Information, Figure S1).

Characterization. TEM. Transmission electron microscopy (TEM) images were recorded using a FEI Tecnai 20 instrument equipped with a Gatan camera.

HRTEM. High resolution TEM (HRTEM) images and scanning TEM (STEM) images were recorded using an FEI Titan 300 keV Cs corrected microscope at the CCEM facility at McMaster University.

SEM. Scanning electron micrographs were obtained from a Hitachi S-5200 instrument equipped with an Oxford Instruments Inca EDX system. EDX analysis was carried out in the line scan mode.

PXRD. Powder X-ray diffraction (PXRD) measurements were carried out on a Siemens D5000 diffractometer using a high-power Cu KR source operating at 50 kV and 35 mA with a Kevex solid-state detector. A step scan mode was used for data collection with a step size of 0.02 deg and time of 2.0 s per step.

Elemental Analysis. The S and Se atomic element content of the samples was measured via Inductively Coupled Plasma Atomic Emission Spectroscopy (ICP-AES), using a Perkin-Elmer Model Optima 7300DV ICP AEOS spectrometer. The sample was digested in a concentrated acid solution, HCl/HNO_3 3:1 (v/v).

Absorption and Emission. Absorption spectra were obtained on a CARY 100 BIO UV−vis spectrophotometer, whereas a CARY Eclipse Fluorescence Spectrophotometer was used to measure emission spectra at room temperature. All samples were measured in toluene.

Results and Discussion

Multicomponent nanoparticles present a new frontier in nanocrystal synthesis. Hybrid nanocrystals composed of two or more materials joined in various architectures to form unique particles could perform multifunctional tasks based on the specific properties characteristic for each domain. For example, colloidal nanoparticles have been synthesized that can both fluoresce and be responsive to magnetic fields, providing multiple imaging opportunities when studied in biomedical systems.[45] Original heterostructure nanoparticles were prepared by deposition of a shell comprised of a second inorganic material onto the preformed inner nanocrystal core. The resulting onion-like heterostructure is referred to as a core/shell system. Formation of a large heterojunction interface in those hybrid particles typically requires a very good match of lattice constants of the two constituent materials and further manipulation of synthetic parameters which allows for the interfacial energy to be kept low. The requirement for strict lattice matching and minimization of lattice strain narrows the material selection that can coexist in one heterostructure and also limits the thickness of the shell to a few monolayers, as additional strain on the heterojunction and consequently the formation of crystallographic defects is induced with each

(45) Choi, J. S.; Jun, Y. W.; Yeon, S. I.; Kim, H. C.; Shin, J. S.; Cheon, J. *J. Am. Chem. Soc.* **2006**, *128*, 15982.

additional monolayer of shell material. However, alternative heterostructure formation mechanisms have taken advantage of lattice mismatching, and, more recently, bifunctional composite nanostructures have been prepared by taking advantage of lattice mismatching in conjunction with selective annealing to generate heterodimers of nanoparticles.[46,47]

A second generation of nanoheterostructures is based on the implementation of anisotropic nanocrystals as a platform for the growth of a secondary material. Those structures can possess a higher complexity in their compositional materials as well as the architectural distribution of the various phases that constitute the heterostructure. Strain does not pose limitations in their formation as previously observed in spherical geometries based on a concentric architectural assembly of different domains. Formation of anisotropic nanocrystals has been best documented in cadmium chalcogenide systems, where superb control over the geometric parameters of one-dimensional nanostructures has been demonstrated.[48,49] The inherent wurtzite crystal phase exhibited by those materials under certain thermodynamic conditions in addition to suitable surfactant molecules which allow for modulation of the surface energies of exposed crystal phases represent ideal conditions for the one-dimensional growth evolution of nanorods. Wurtzite nanoparticles when formed in the presence of suitable ligands exhibit variation in the polarity of their lateral and basal facets. Much slower growth rates have been noted for the lateral, nonpolar facets, as supposed to the basal, polar facets, accentuating the preferential expansion of nanorods along their unique *c* axis. Consequently, the higher reactivity of the tips of such cadmium chalcogenide anisotropic nanoparticles allows for site-specific nucleation of a second material in the formation of 1D dumbbell heterostructures. Furthermore, the absences of a plane of symmetry perpendicular to the *c* axis in wurtzite nanorods leads to the nonequivalence of the 001 and $00\bar{1}$ tips and significant differences in the growth rates along those two directions, as was recently also confirmed through ab initio calculations.[50] This concept was strategically implemented by Kudera et al.[21] and Mokari et al.[22] as they successfully manipulated the synthetic conditions and demonstrated controlled nucleation of either a second semiconductor or metallic material which was either localized to one or both of the tips of the original one-dimensional wurtzite nanocrystal, leading to the formation of matchstick- or dumbbellshaped heterostructures.

Synthesis of heterostructures through single source precursor thermolysis is very rare and has only been reported for CdS-ZnS nanowires that were prepared using the one-step metallo-organic chemical vapor deposition (MOCVD) process with cofed single-source precursors.[51,52] Also, the solution-liquid−solid growth method has been implemented in the fabrication of metal sulfide particles with catalyst nanoparticles tips via the thermal decomposition of single-source precursors.[53,54]

For solution phase routes one would expect the typical challenges encountered in shape control when single-source precursors are employed also to be problematic for heterostructure formation from those compounds. One of the key limiting parameters is the temperature required for the decomposition of the single-source precursor, which ultimately dictates also the temperature of the deposition of the secondary material onto the preformed seed nanoparticles. Here, we have prepared bifunctional composite nanostructures through a two step synthesis, by selectively growing spherical EuS nanocrystals on the tips of CdSe (Figure 1c-e) and CdS nanorods (Figure S1). An eight-coordinate lanthanide based single-source precursor, $Eu(Ddtc)_3(Bipy)$, previously used in the preparation of monocomponent EuS nanoparticles (Figure 1a),[38,39] was used as the material source for the growth of EuS domains. The decomposition temperature of this molecular precursor has been noted to be in the range of 280 °C−290 °C in the presence of a surfactant mixture including oleylamine and octadecene. The high reaction temperature is not ideal for the deposition of the second material but could not be avoided as the decomposition of the europium based precursor preceded the growth of the EuS domains.

Dropwise addition of a slurry of $Eu(Ddtc)_3(Bipy)$ in oleylamine into the solution of preformed CdSe nanoparticles (Figure 1b) resulted in the formation of EuS-CdS heteronanocrystals (Figure 1c). A number of morphological and compositional changes were noted during the formation of these novel nanoparticles. The growth of EuS domains coincided with the anion replacement in the CdSe nanorod components of the hybrid particles. The high temperature required for the decomposition of the $Eu(Ddtc)_3(Bipy)$ precursor in conjunction with the excess sulfur available as a result of the breakdown of the diethyldithiocarbamate ligand and the excess cadmium used in the synthesis of original CdSe nanorods promoted conditions conducive to anion displacement in CdSe domains and the formation of "CdS stems". SEM micrographs of the resulting structures are shown in Figure 1d-e, illustrating the heterogeneous composition of the nanoparticles.

The compositional cross-section along the long axis in Figure 1d illustrates the localization of europium at the tips of the heterostructure and the distribution of cadmium in the central domain. Sulfur, on the other hand, is seen as the dominant chalcogenide throughout the whole structure and the presence of selenium appears to be minimal and on the order of that of titanium, which does not appear in the particle and was purely used for a baseline comparison. The

(46) Gu, H; Zheng, R.; Zhang, X.; Xu, B. *J. Am. Chem. Soc.* **2004**, *126*, 5664.
(47) Zhang, J.; Tang, Y.; Lee, K.; Ouyang, M. *Science* **2010**, *327*, 1634.
(48) Peng, X. G.; Manna, L.; Yang, W. D.; Wickham, E.; Scher, E.; Kadavanich, A.; Alivisatos, A. P. *Nature* **2000**, *404*, 59.
(49) Manna, L.; Scher, E. C.; Alivisatos, A. P. *J. Am. Chem. Soc.* **2000**, *122*, 12700.
(50) Puzder, A.; Williamson, A. J.; Zaitseva, N.; Galli, G.; Manna, L.; Alivisatos, A. P. *Nano Lett.* **2004**, *4*, 2361.
(51) Hsu, Y.-J.; Lu, S. Y. *Chem. Commun.* **2004**, 2102.
(52) Barrelet, C. J.; Wu, Y.; Bell, D. C.; Lieber, C. M. *J. Am. Chem. Soc.* **2003**, *125*, 11498.
(53) Yu, H.; Li, J.; Loomis, R. A.; Wang, L.-W.; Buhro, W. E. *Nat. Mater.* **2003**, *2*, 517.
(54) Sun, J.; Buhro, W. E. *Angew. Chem., Int. Ed.* **2008**, *47*, 3215.

cross section along the short axis of the "stem" portion of the heterostructures (Figure 1e) confirms the displacement of selenium and uniform incorporation of sulfur throughout the initial CdSe domain. The material changes of the nanorod region during the addition of EuS are accompanied by a morphological evolution. The nanoparticles undergo a thickening process and their length distribution is somewhat broadened.

The exposure of the preformed nanorods to high temperature conditions, in addition to the modulation of the surfactant mixture, are believed to be conducive to triggering ripening processes and the resulting shape transformation. A control experiment, where preformed CdSe nanorods were subjected to simulated conditions of heterostructure growth — heating to high temperatures in the presence of oleylamine (without the addition of EuS precursor) — produced CdSe nanorods whose absorption as a result of the increase of their short axis is considerably red-shifted compared to the parent CdSe particles (Figure S2a-c). It is not surprising that high temperature conditions and low precursor influx would promote the transformation of 1D nanostructures into more thermodynamically stable morphologies. Furthermore, control experiments were also run, where in addition to high temperatures and the presence of oleylamine, preformed CdSe nanorods were subjected to the addition of small amounts of EuS precursor. In those trials, no nucleation of EuS was observed, but the anisotropic CdSe particles transformed into shorter nanorods and underwent a compositional change to CdS (Figure S2d-f).

The selective growth of EuS nanoparticles occurred on the tips of the anisotropic CdS(Se) structures, while these conditions also promoted some homogeneous nucleation of EuS nanocrystals in solution. Approximately 15% of the anisotropic particles have EuS spheres on each end, whereas others exhibit secondary domains only on one tip. It was previously suggested that higher temperatures decrease the selectivity in the end-growth,[21] but since the thermolysis of $Eu(Ddtc)_3(Bipy)$ occurs at relatively high temperature, it is hard to avoid this problem.

The material composition of synthesized EuS-CdS(Se) nanocrystals has been confirmed with powder X-ray diffraction (Figure 2). The diffraction spectrum indicates that EuS crystallized in its typical rock-salt structure, cubic *Fm*-3*m* phase (a = 5.962 Å). The cadmium chalcogenide portion of the heterostructure is consistent with a wurtzite phase, *P*-63-*mc*, which matches more closely CdS, than CdSe. Rietveld refinement results of the PXRD data for the EuS/CdS(Se) nanocrystals also suggest a dominant CdS crystal structure and a smaller CdSe crystalline phase (a = 4.166 Å, c = 6.787 Å) (Figure S3). The overwhelming presence of sulfur in the system is also supported by ICP AES data, where the ratio of S:Se was 10:1 in agreement with the EDX line scans in Figure 1d-e, where selenium was hardly detectable.

HRTEM micrographs were able to resolve the atomic structure of the CdS and EuS phases in individual nanocrystals. The structure of the CdS component was in some instances single crystal (Figure 3), with no stacking faults

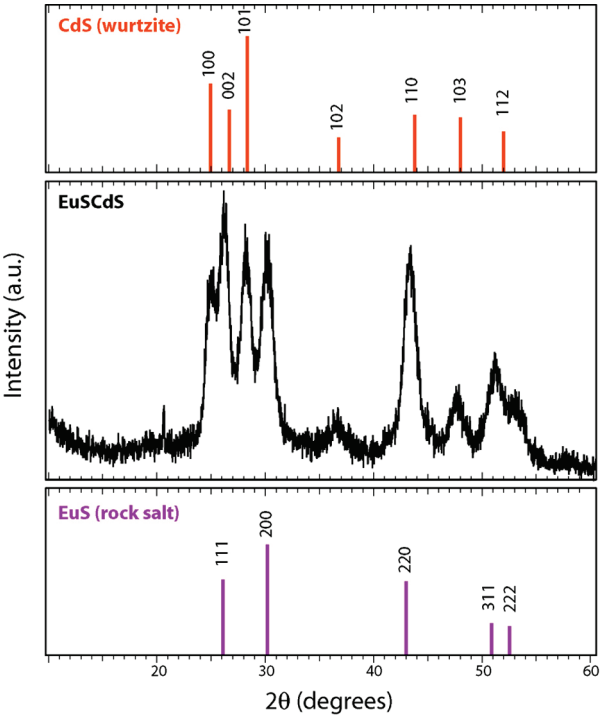

Figure 2. PXRD spectrum of EuSCdS nanoheterostructures compared with the diffraction pattern of bulk wurtzite CdS and rock-salt EuS.

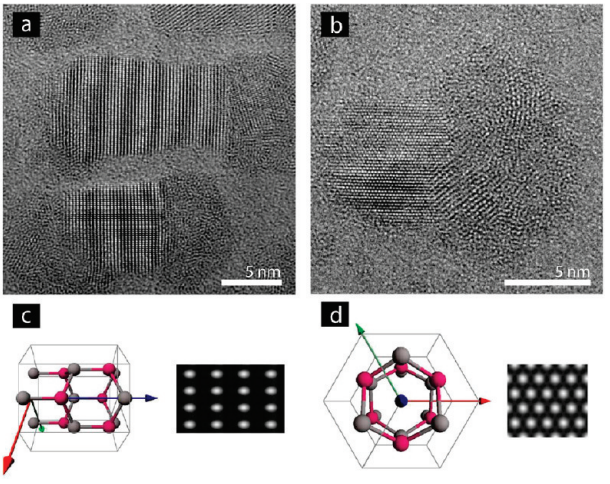

Figure 3. The atomic structure of the CdS domain in a single nanoheterostructure is clearly resolved in the [1$\bar{1}$00] (a) and [0001] (b) crystal zone axis orientation. The HRTEM phase contrast is in good agreement with calculated HRTEM images (c), (d).

or point defects present. In other instances, nanoheterostructures featured a mix of wurtzite and zinc blende structures in the CdS phase (Figure 4). It is important to note that the preformed CdSe nanorods, that were used as the platform for the formation of these nanostructures, displayed a PXRD spectrum indicating a wurtzite structure, implying that the mixture of wurtzite and zinc blende crystal domains in cadmium chalcogenide parts of the heterostructure formed in the second part of the synthesis during the anion exchange process. For the structure in Figure 3a, lattice *d*-spacings of 0.30 and 0.18 nm were measured for the CdS (002) and CdS ($\bar{1}$20) hkl planes, respectively. These are in good agreement with known CdS lattice parameters, where

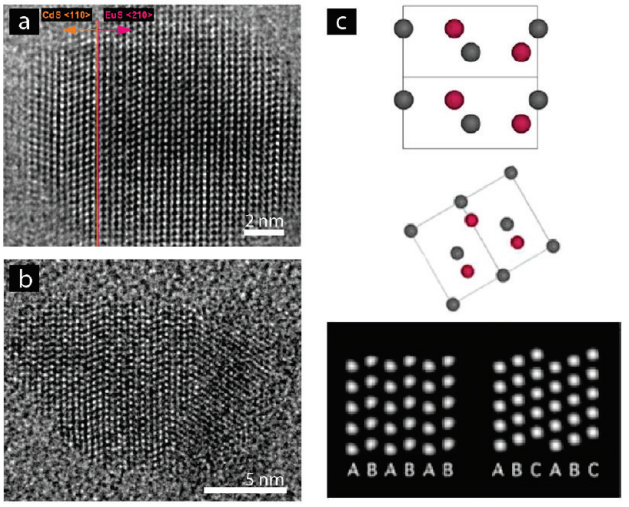

Figure 4. HRTEM images reveal the atomic stacking sequences in the CdS domain of the individual nanoheterostructures. (a) The EuS domain of the nanoparticle is single crystal. The CdS domain has a zinc blende structure (ABCABC) with a twin boundary. (b) Both ABAB and ABCABC stacking sequences, indicative of wurtzite and zinc blende structures, respectively, are present in the CdS domain. (c) The unit cells and corresponding HRTEM image simulations calculated for CdS wurtzite and CdSe zinc blende at 80 nm defocus and 10 nm thickness viewed down the $<uvw>$ = ⟨110⟩ zone axis. The CdSe 'dumbbells' are not resolved in the simulations for the imaging conditions used.

d(002)/d($\bar{1}$20) = 1.62.[55] In Figure 4(a) crystallographic planes were indexed, and spacings were measured for both CdS and EuS domains in a single heterostructure with the aid of the Fourier transform. CdS(11$\bar{1}$) and CdS (20$\bar{2}$) planes have a measured spacing of 3.2 Å and 2.1 Å, respectively. The EuS (002) and EuS ($\bar{1}$20) planes have a measured lattice spacing of 4.1 Å and 2.6 Å, respectively. Simulated HRTEM images of CdS for the both wurtzite and zinc blende structures viewed down the ⟨110⟩ zone axis show strong resemblance to the observed CdS structures (Figure 4c) [images simulated with JEMS (image simulation program developed by P. Stadelmann, EPFL, Lausanne)]. The crystallinity of the EuS phase is also detected in Figure 4.

It was previously observed by Mokari et al.[20] that gold domains showed no preferential crystallographic orientation with respect to the cadmium chalcogenide wurtzite substrate particles. On the other hand, PbSe extensions that evolved on the tips of CdS or CdSe nanorods preferentially grew along the ⟨002⟩ direction of the rock salt phase, which was aligned with 100 planes of CdS and CdSe wurtzite.[21] It was possible to derive the heteroepitaxial relationship between CdS and EuS, as both of the lattices were resolved, demonstrating a CdS ⟨110⟩/EuS ⟨210⟩ orientation relationship (Figure 4a). The heterojunction is atomically sharp as evidenced in Figure 4a by the direct observation of change in atomic structure across the junction. The sharp junction is also evident in HAADF STEM images (Figure 5b) by the distinct change in contrast across the junction. The higher intensity (scattering) from atomic columns in the EuS domain is a result of the stronger electron scattering power from the heavy Eu nucleus. The majority of nanoparticles displayed small

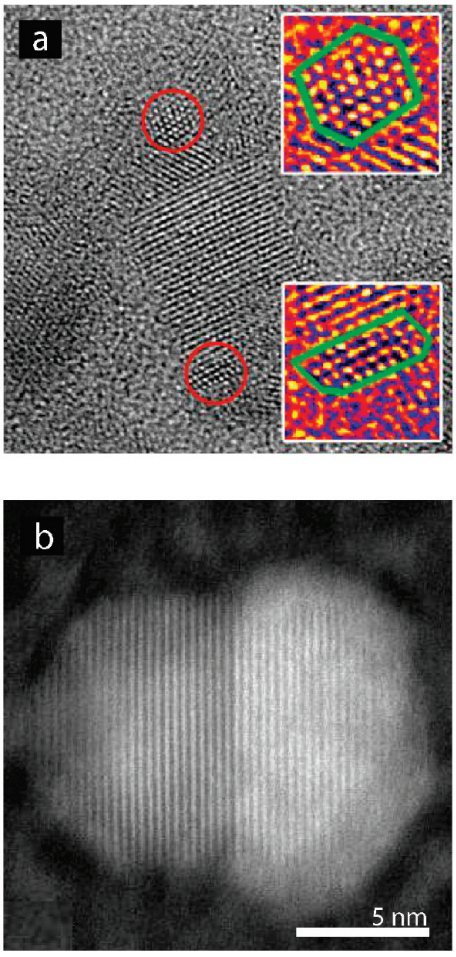

Figure 5. (a) Small regions of atomic ordering are observed in the EuS phase. (b) A sharp, planar interface divides the CdS phase from the EuS phase in the HAADF STEM image.

regions of crystalline order in the EuS phase (Figure 5a). In such cases, the EuS lattice may be partially covered by an organic ligand surface coating, generating amorphous contrast and obscuring the underlying ordered lattice. High angle annular dark field (HAADF) STEM images clearly distinguish the EuS and CdS phases in individual nanocrystals, featuring comparatively high and low intensity for each phase, respectively (Figure 5b). The EuS phase is a stronger scatterer than CdS at high angles in accordance with the general rule $I \propto Z^2$ for HAADF STEM images. The HAADF STEM images also reveal sharp, planar EuS/CdS interfaces (Figure 5b).

Absorption and emission experiments, summarized in Figure 6, were carried out to study the effect of EuS growth on the optical properties of the cadmium chalcogenide nanorods. The original CdSe nanorods absorb at 600 nm, whereas their emission is positioned at 611 nm. The absorption spectrum of monocomponent EuS cubes (10 nm) is also shown in Figure 6a for a comparison. EuS was found to exhibit bulk behavior on the nanoscale, in accordance with the estimated electron and hole Bohr radii, which are less than 1 nm.[56] The band in the visible is attributed to the $4f^7$-$5d$ t_{2g} transition in

(55) Ballentyne, D. W. G.; Ray, B. *Physica* **1961**, *27*, 337.

(56) Chen, W.; Zhang, X. H.; Huang, Y. N. *Appl. Phys. Lett.* **2000**, *76*, 2328.

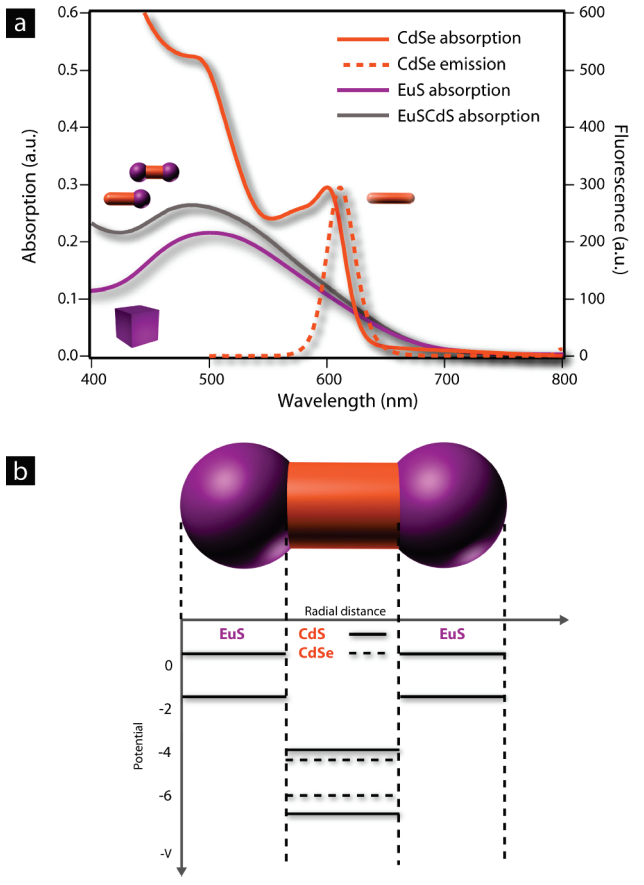

Figure 6. (a) Preformed CdSe nanorods (Figure 1b) which absorb around 600 nm are highly emissive, but upon the addition of EuS caps, the absorption shifts to the blue coinciding with the absorption of EuS and CdS. EuS-CdS heterostructure show no fluorescence. (b) Schematic diagram of conduction and valence band edges for a EuS-CdSe/CdS heterostructure constructed from bulk value. The heterojunction is type III, with a characteristic broken band gap line-up.

bulk EuS.[39,57,58] The absorption features of the resultant EuS-CdS heterostructure appear to be dominated by the EuS component with a broad peak centered around 500 nm. The contribution from the cadmium chalcogenide phase is only visible as increased absorption of the heterostructure below 500 nm as compared to pure EuS nanocrystals. The featureless contribution of CdS in the absorption spectrum of the heterostructure is similar to the mildly sloping offset observed for the CdS nanorods formed from CdSe nanocrystals (Figure S2d-f). Similar observations have also been made following the growth of EuS tips on prefabricated CdS nanorods (Figure S1b). The initial absorption of CdS, manifested as a shoulder at 450 nm, is still evident as a feature in the absorption spectrum of the EuS-CdS heterostructure, which also displays a broad shoulder between 500 and 600 nm attributed to EuS absorption.

Figure 6b shows the alignment of the conduction and valence band edges of the two materials constituting the hybrid structure. This band arrangement is not as typical as type I and type II, which are more commonly encountered in hybrid structures, but rather represents the unusual case of type III (type IIb misaligned), or broken-band alignment, such as in GaSb-InAs heterostructures.[59,60] In the broken-gap heterojunction, the conduction band bottom of CdS lies below the valence band top of EuS, illustrating the possibility of the population of the CdS conduction band from the valence band states of EuS. In heterostructures the emission is completely quenched, as was also the case for Au-CdSe nanodumbbells, where the original emissive properties of the CdSe nanorod were lost when Au domains were grown at their tips.[20] We believe that the conduction band of CdS can be populated by EuS valence states through wave function leakage, leading to band filling or quasi band filling. Certainly, excitations in the CdS would be quenched by EuS due to differences in excitation energies.[61,62] Incorporation of insulating domains might be necessary in order to preserve the emissive properties of CdSe nanorods when they are integrated in such hybrid multicomponents structures, which certainly would complicate synthetic procedures.

Conclusions

The structure and properties of EuS nanocrystals have been extended through the preparation of EuS-CdS heterostructures. The crystallographic properties of these two semiconductor materials, which possess a poor lattice match, favored the production of dumbbell-like hybrid particles with an epitaxial relationship CdS ⟨110⟩/EuS ⟨210⟩. These unique nanoheterostructures display an unusual band alignment belonging to the type III (type IIb) class heterojunctions, characterized by the broken band alignment. Preliminary results on their optical properties suggest that the emission of the CdS rod component is quenched in the presence of EuS spheres on its tips. It would be interesting to explore the architectural tunability of this hybrid structure and its effects on the collective optical and magnetic properties of EuS-CdS nanocrystals. Although limited in terms of possible reaction parameters, this EuS system is an interesting example of a high-temperature thermolysis single-source precursor method, whose exploration might provide valuable information for the design of a general growth model for heteronanocrystals.

Acknowledgment. The Natural Sciences and Engineering Research Council of Canada is gratefully acknowledged for support of this research. The authors thank Dr. Srebri Petrov for PXRD analysis, Dr. Neil Coombs for SEM micrographs, and Dan Mathers for ICP AES analysis and the Canadian centre for electron microscopy (CCEM) at McMaster University for HRTEM and STEM imaging.

Supporting Information Available: Additional characterization and experimental details including structural and photophysical characterization; UV−vis, TEM and PXRD data. This material is available free of charge via the Internet at http://pubs.acs.org.

(57) Narayanamurti, V. *J. App. Phys.* **1971**, *42*, 1369.
(58) Güntherodt, G. *Phys. Condens. Matter* **1974**, *18*, 37.
(59) Mikhailova, M. P.; Moiseev, K. K; Voronina, T. I.; Lagunova, T. S.; Yakovlev, Yu. P. *Semiconductors* **2007**, *41*, 161.
(60) Beerens, J.; Gregoris, G.; Portal, J. C.; Mendez, E. E.; Chang, L. L.; Esaki, L. *Phys. Rev. B* **1987**, *36*, 4742.
(61) Scholes, G. D.; Andrews, D. L. *Phys. Rev. B* **2005**, *72*, 125331.
(62) van der Meer, B. W.; Coker Ill, G.; Chen, S.-Y. *Resonance Energy Transfer: Theory and Data*; VCH Publishers Inc.: New York, 1994.
(63) Talapin, D. V.; Nelson, J. H.; Shevchenko, E. V.; Aloni, S.; Sadtler, B.; Alivisatos, A. P. *Nano Lett.* **2007**, *7*, 2951.